Terahertz emission and spectroscopy on InN epilayer and nanostructure

H. Ahn*[a], C.-L. Pan[a], and S. Gwo[b]
[a]Department of Photonics and Institute of Electro-optical Engineering, National Chiao Tung University, Hsinchu 30010, Taiwan, Republic of China; [b]Department of Physics, National Tsing Hua University, Hsinchu 30013, Taiwan, Republic of China

ABSTRACT

We report a comprehensive study on THz emission and spectroscopy of indium nitride (InN) films and its nanorod arrays grown by plasma-assisted molecular beam epitaxy technique. For the enhancement of THz emission from InN, we demonstrated two method; firstly using nanorod arrays, which have large surface area for optical absorption and THz emission, and secondly using nonpolar InN film, of which the electric field is along the sample surface. We propose that a "screened" photo-Dember effect due to narrow surface electron accumulation layer of InN is responsible for the nanorod-size-dependent enhancement from InN nanorods. The primary THz radiation mechanism of nonpolar InN is found to be due to the acceleration of photoexcited carriers under the polarization-induced in-plane electric field. THz time-domain spectroscopy has been used to investigate THz conductivity and dielectric response of InN nanorod arrays and epitaxial film. The complex THz conductivity of InN film is well fitted by the Drude model, while the negative imaginary conductivity of the InN nanorods can be described by using a non-Drude model, which includes a preferential backward scattering due to defects in InN nanorods, or a Coulombic restoring force from charged defects.

Keywords: Indium Nitride, nanostructures, THz emission, THz time-domain spectroscopy, non-Drude model

1. INTRODUCTION

Since its recent discovery of narrow band-gap and the superior electron transport properties over other group-III nitrides, indium nitride (InN) has emerged as a potentially important semiconductor for use in near-infrared (NIR) optoelectronics and high-speed electronics.[1-5] Recently measured high optical absorption of InN in the NIR range of the solar spectrum is several orders of magnitude larger than Si and it opens the potential of InN for thin-film solar cell applications.[6,7] Furthermore, InN not only has a narrow band-gap, but also has remarkably large energy-gap (~ 2.8 eV) between the conduction band minimum and the next local minimum of InN so that undesired energy transition of photoexcited carriers to the local minimum can be minimized. The high electron mobility and high energy-gap to local minimum inspire potential applications of InN in the terahertz (THz) range application, for example as an efficient THz emitter/detector.[8-11]

Recently, low-dimensional InN nanomaterials in the forms of nanowires, nanorods, nanotubes, etc. have received great attention due to their potential in the development of highly efficient optoelectronic devices and photovoltaic applications. Vertically aligned InN nanorod arrays grown on silicon by plasma-assisted molecular beam epitaxy (PAMBE) are known to possess the crystal properties similar to wurtzite InN single crystal.[12,13] The size distribution and the aerial (coverage) density of nanorods can be engineered by the growth conditions. It has been suggested that enhanced electron accumulation at the surface of the InN nanorods due to the high surface-to-volume ratio makes InN nanorod arrays a promising material for NIR sensor applications. Meanwhile, to realize the prospect of THz applications, it is essential to understand fundamental THz properties of InN. Knowledge of dielectric functions in GHz-THz range is particularly important for devices operating in the far-infrared range since material-THz wave interaction can affect the performance of devices. To date, relatively few studies have explored InN in THz range and even fewer is reported for low-dimensional InN nanostructures. The critical material properties in THz range, such as complex THz conductivities and dielectric responses of a specimen can be measured by a contactless method, THz time-domain spectroscopy (THz-TDS). In particular, THz-TDS is proved to be a novel tool to deduce the material properties of nanostructured materials which cannot be measured by the conventional method, such as electron Hall measurement to measure the mobility.

*hyahn@mail.nctu.edu.tw; phone 886 3 5712121-56369; fax 886 3 5716631

Gallium Nitride Materials and Devices IV, edited by Hadis Morkoç, Cole W. Litton, Jen-Inn Chyi, Yasushi Nanishi, Joachim Piprek, Euijoon Yoon, Proc. of SPIE Vol. 7216, 72160T
© 2009 SPIE · CCC code: 0277-786X/09/$18 · doi: 10.1117/12.805546

Typical light emitting sources regardless of whether operating in the optical range or in THz range suffer the fundamental problem of low light extraction efficiency due to the total internal reflection in a material of high refractive index. This is also one of the central issues in manufacture of highly bright light emitting devices (LED). Therefore, it is natural to seek for the materials or the methods which can provide the larger surface areas for internal radiation to easily escape from the surface. Nanostructured materials, such as nanocolumns and nanowires, are suggested to increase the effective surface areas due to their large surface-to-volume ratios. Increase of light coupling through a prism is also practiced to reduce the refractive index difference between the ambient and the THz emitting materials.[14] We investigated the THz emission and power enhancement mechanism in InN nanorods with different sizes. Since the THz emission from InN depends on the acceleration of electrons in the proper electric field, externally applied strong magnetic field can be used to rotate the direction of dipole oscillation to coincide with the small emission cone and enhance the power of THz emission.[15-17] In this paper, we introduce a new method to enhance the THz radiation by simply using the InN film grown along the nonpolar direction.

2. EXPERIMENTAL METHOD

2.1 Experimental set-up

Figure 1(a) shows schematically our experimental set-up for THz-TDS measurement based on the low-temperature-grown GaAs (LT-GaAs) photoconductive (PC) dipole antennas which are used for generation and detection of THz pulses. A Ti:sapphire laser system with the repetition rate of 80 MHz at the center wavelength of 800 nm is used for the excitation of PC antennas. The normally transmitted THz pulses were measured by another PC antenna as a function of delay time with respect to the optical probe pulse. Fig. 1(b) shows the experimental set-up to measure the THz emission from the samples. In this set-up, the samples were photoexcited by an obliquely incident laser pulses from an amplified Ti:sapphire laser system, which delivers the laser pulses at a center wavelength of 800 nm and of 50 fs duration. The photoexciting beam is collimated on the samples with a spot size of ~ 2 mm at the angle of incidence of 70˚, which is near the Brewster angle. The transient photoexcitation initiates coherent plasma oscillations of the photoexcited carriers in the samples, which leads to the emission of few-cycle THz pulses. The THz pulses are measured by a time-resolved technique in a 1 mm-thick ZnTe crystal, where the Pockels effect due to the THz field rotates the polarization of the sampling laser pulses. A balanced detector detects the differential photocurrent as a function of time delay between the THz pulses and optical probe beam. All the measurements were done under dry nitrogen purge.

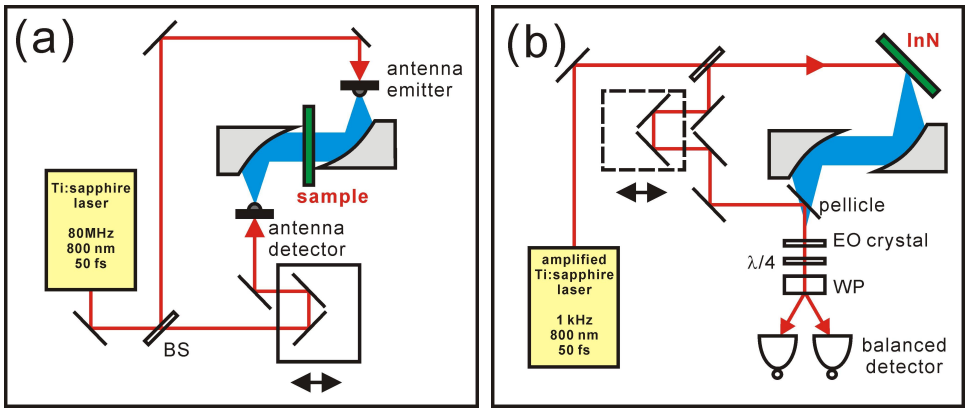

Fig. 1. (a) The experimental set-up for the THz time-domain spectroscopy. The major part of laser pulses are delivered to a photoconductive antenna for THz emission and relatively weak laser pulses are used as the probe beam with time delay. Two parabolic mirrors are used for collection and collimation of the generated THz pulse and the samples were placed in the way of collimated THz beam. (b) The experimental set-up for the measurement of THz emission from the semiconductor surfaces. The strong photo-exciting pulses are incident on the sample at the angle of 70˚. The terahertz pulses were detected by free-space electro-optic sampling in a 2-mm-thick ZnTe crystal as a function of delay time with respect to the optical pump pulse.

The morphologies and size distribution of InN nanorods were analyzed using field-emission scanning electron microscopy (FE-SEM). We have also investigated the azimuthal angle dependence of THz emission from *c*- and *a*-plane InN films. At high pump rate, nonlinear effect-induced THz emission from the semiconductor surfaces shows the characteristic azimuthal angle dependence.

2.2 Sample preparation

For this work, two of InN epitaxial films grown along the different growth axis and two of InN nanorod films grown at different sample temperatures were prepared by PAMBE. To relax the heterointerface lattice mismatch, a wurtzite InN epitaxial film grown along the *c*-axis (*c*-plane InN) was grown on Si(111) using the epitaxial AlN/β-Si_3N_4 double-buffer layer technique.[13] The vertically-aligned InN nanorods were grown at sample temperature of 330°C (low-temperature grown nanorods, LT-NR) and 520°C (high-temperature grown nanorods, HT-NR) on β-Si_3N_4/Si(111) (without the AlN buffer layer).[12] The N/In flux ratios were ~ 2.6 and ~ 6.0 for LT-NR and HT-NR, respectively. The thicknesses of the InN epilayer, LT-NR, and HT-NR are ~ 2.5 μm, 750 nm, and 700 nm, respectively. In the meantime, the InN film grown along the *a*-axis (*a*-plane InN) (~1.2 μm) was grown on an *r*-plane {1-102} sapphire wafer. Fig. 2(a) and (b) show the SEM images of *a*-plane InN film. The growth direction of the InN film was determined using a 2θ–ω x-ray diffraction scan. The in-plane epitaxial relationship between *a*-plane InN and *r*-plane sapphire is $[0001]_{InN} \| [-1100]_{Al2O3}$ and $[-1100]_{InN} \| [11-20]_{Al2O3}$.[18] Near-infrared photoluminescence (PL) was detected from the as-grown *a*- and *c*-plane InN films and LT- and HT-NR at room temperature. Particularly, room-temperature PL signals of HT-NR and LT-NR are about one to two orders of magnitude lower than that of the InN film.[12] Unintentionally doped *n*-type carrier concentrations of 7.0×10^{18} and 3.1×10^{18} cm^{-3} and electron mobilities (μ) of 298 and 1036 cm^2/Vs were determined by room-temperature Hall effect measurements for *a*- and *c*-plane InN films, respectively.

The SEM image of the hexagonal-shaped LT-NR in Fig. 2(c) exhibits nanorods with a uniform diameter of ~130 nm, while that of the HT-NR shown in Fig. 2(d) reveals that besides the large-size nanorods, there are ultra-small nanorods with an average diameter of ~60 nm filling up the spaces between larger-size (~ 130 nm) nanorods. The LT-NR exhibits an average aspect ratio (height/diameter) of ~ 6 and an aerial density of ~ 5×10^9 cm^{-2}. The average aspect ratio of the HT-NR is ~ 5.4 and ~ 12 for large and small nanorods, respectively and the aerial density of HT-NR is ~ 8×10^9 cm^{-2}, including both large and ultra-small rods.

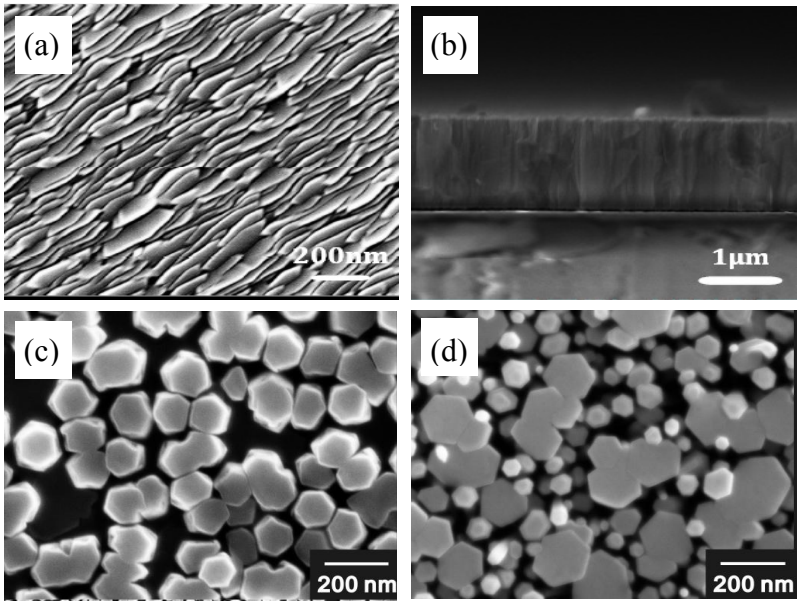

Fig. 2. The top (a) and side view (b) of *a*-plane InN imaged by the SEM. The top view shows the directional growth of *a*-plane InN. From the side view, the thickness of film is determined to be 1.2 μm. SEM images of vertically aligned (c) low-temperature-grown nanorods (LT-NR) and (d) high-temperature-grown InN nanorods (HT-NR), grown on Si(111) substrates by nitrogen-plasma-assisted molecule beam epitaxy. LT-NR has a uniform radius of 65 nm, while that of the HT-InN nanorods reveals a bimodal size distribution.

3. SPECTROSCOPIC STUDIES OF NANOSTRUCTURES

3.1 Frequency-dependent dielectric functions of *c*-plane InN film

In THz-TDS analysis, the THz waveform is obtained by measuring the average photocurrent as a function of time delay between the THz pulses and the gating optical pulses. From a Fourier analysis of measured THz pulses, the amplitude and phase of frequency-dependent THz response can be obtained so that the uncertainty caused by the Kramers-Kronig analysis can be avoided. Since THz spectra reflect the charge carrier behavior in the materials, the material properties, such as complex dielectric constants can be describe by the Drude model. The measured time-domain THz waveforms from InN film, InN nanorods, and the reference material, Si(111) substrates are Fourier transformed into the complex amplitude in the frequency domain. From the experimentally measured spectral amplitude and the phase difference between the samples and the substrate, the frequency-dependent refractive index of *c*-plane InN film is calculated through the iterative fitting. Figure 3(a) shows the calculated real (solid circles) and imaginary (open circles) parts of the frequency-dependent refractive index ($\tilde{n} = n + ik$) of the InN film. Both *n* and *k* decrease monotonically with increasing frequency and close values of *n* and *k* over the spanning spectral range reflects the free-electron-like behavior of charge carriers. The complex dielectric constant is related with the refractive index and the conductivity by

$$\varepsilon(\omega) = \varepsilon_\infty + i\frac{\sigma(\omega)}{\omega\varepsilon_0} = (n+ik)^2, \tag{1}$$

where ε_0 is the permittivity of free space, $\sigma(\omega)$ is the complex conductivity, and the dielectric constant ε_∞ is 6.7 for InN.[19] From the deduced frequency dependent conductivity shown in Fig. 3(b), we find the real part of conductivity, Re[σ] is monotonically decreasing as the frequency increases, while Im[σ] increases slowly. This frequency dependence is typically observed for Drude-like materials below the plasma frequency. We thus fit the measured complex refractive index and conductivity in Fig. 1 using the simple Drude model,[5] in which the complex conductivity is defined by

$$\sigma(\omega) = \frac{\varepsilon_0\omega_p^2\tau_0}{1-i\omega\tau_0}, \tag{2}$$

where $\omega_p = \left(Ne^2/m^*\varepsilon_0\right)$ is the plasma frequency and τ_0 is the carrier scattering time. From the best fit to the experimental data we obtained $\omega_p/2\pi$ = 52±1.2 THz and τ_0 = 52±2.5 fs. We assume that an electron effective mass of the InN film is $m^* = 0.075\,m_0$ [4] and then obtained the corresponding carrier density $N = \omega_p{}^2 m^* \varepsilon_0 / e^2 = 2.5\pm0.2\times10^{18}$ cm^{-3} and a carrier mobility $\mu = e\tau_0 / m^*$ =1217±58 cm^2/Vs. These values are in an excellent agreement with the separately measured room-temperature Hall effect measurement results of 3.1×10^{18} cm^{-3} and 1036 cm^2/Vs, respectively.

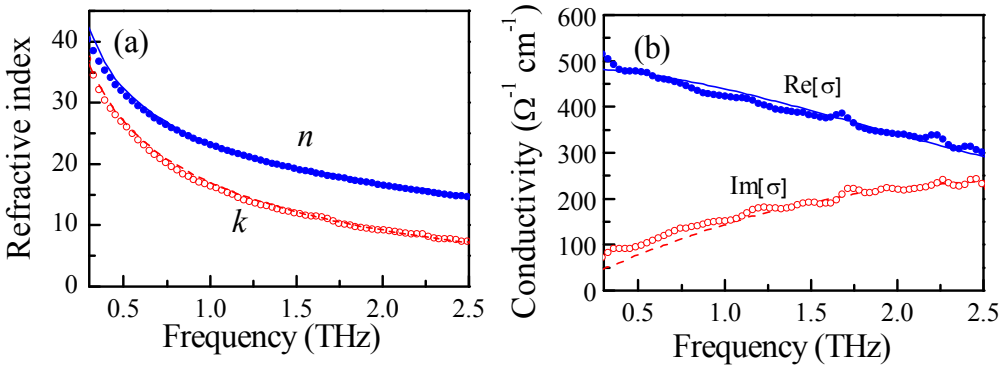

Fig. 3. (a) Complex refractive index of InN film as a function of frequency. The solid and dashed lines are obtained by the best fit to the data based on the Drude model. (b) Corresponding complex dielectric constant of InN film calculated by equation (1) in the text.

3.2 Frequency-dependent dielectric functions of *LT-NR*

For the THz spectroscopic study of InN nanorods, due to the complexity of the structures of HT-NR (including both large and small sizes of nanorods), we only studied LT-NR with a uniform size of nanorods. Furthermore, HT-NR is nearly transparent to the incident THz pulses so that it was difficult to get the differential transmittance of HT-NR to analyze its optical properties in the THz range. Meanwhile, THz pulses were highly absorbed in LT-NR, similar to InN film. The reason for the extremely high THz transmission for HT-NR is not clear yet. Since the InN nanorod film is consisted of loosely packed InN nanorods and air, it is necessary to extract the sole contribution of nanorods to the optical properties. Therefore, we first applied the effective medium approximation (EMA)[20] to obtain the dielectric functions of the pure InN nanorods, which is described by

$$\varepsilon_{eff}(\omega) = f\varepsilon_m(\omega) + (1-f)\varepsilon_h, \tag{3}$$

where $\varepsilon_m(\omega)$ and ε_h are the dielectric constants of the pure InN nanorods and the host medium, air and f is the filling factor. From the SEM image shown in Fig. 1, we obtained $f \sim 0.7$ for LT-NR. Figure 4(a) and (b) illustrate frequency-dependent refractive index and complex conductivity of the pure InN nanorods extracted under EMA, respectively. Monotonic decrease of the complex refractive index of the nanorods is similar to that of InN film and even closer values of n and k show more metallic behavior of carriers in nanorods. Meanwhile, the complex conductivity response of the nanorods is quite different from that of InN film. For InN nanorods, Re[σ] is gradually increasing with increasing frequency, while Im[σ] is decreasing with increasing frequency with a negative value over the whole scanning frequency range. This peculiar frequency dependence is a typical behavior of low-dimensional materials, which commonly show negative and gradually decreasing Im[σ]. To explain this non-Drude-like behavior of low-dimensional materials, Smith recently proposed a modified Drude model (we will it as Drude-Smith model),[21] of which the large fraction of backward scattering of electrons are considered. The complex conductivity in the Drude-Smith model is given by[21]

$$\sigma(\omega) = \frac{Ne^2\tau_0/m^*}{1-i\omega\tau_0}\left[1+\sum_j \frac{c_j}{(1-i\omega\tau_0)^j}\right] \tag{4}$$

where c_j is a parameter describing fraction of the electron's original velocity after some number j of scattering events. In practice, we take only the first term in c_j [$c_1 = c$] and then c varies between –1 and 0, corresponding to Drude conductivity for $c = 0$ and complete backscattering for $c = -1$.

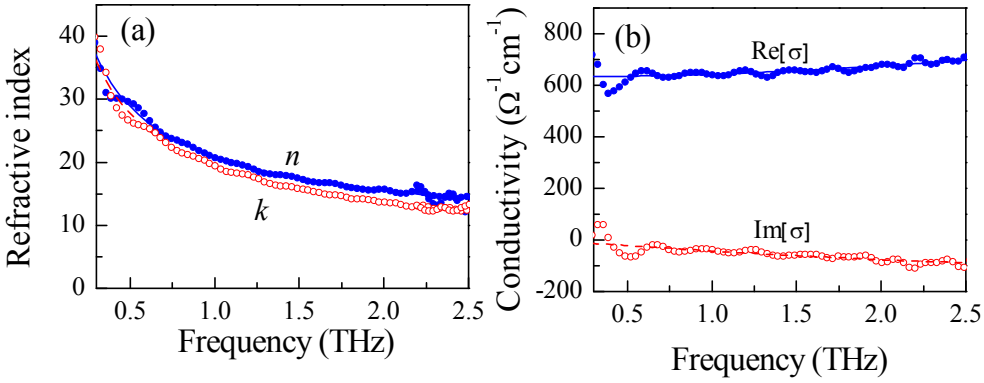

Fig. 4. (a) Complex refractive index of InN nanorods as a function of frequency. The solid and dashed lines are obtained by the best fit to the data based on the Drude-Smith model. (b) Corresponding complex dielectric constant of InN nanorods.

Based on the Drude-Smith model, an excellent fit of complex conductivity of the InN nanorods is obtained with the fit parameters $c = -0.65\pm0.01$, $\tau_0 = 13\pm0.2$ fs, and $\omega_p/2\pi = 199\pm3$ THz. The carrier scattering time τ_0 for nanorods (13

fs) is much smaller than that of InN film (52 fs) due to the larger defect density. Since the obtained plasma frequency 199 THz lies in the near-infrared range, we performed near-infrared reflectivity measurement of InN film and nanorods. Figure 5 shows the results measured at the wavelength covering from 800 nm to 2400 nm. The oscillating behavior of reflectivity of InN film is due to the interference of light within the thin film in the transparent region below the bandgap energy. Meanwhile, the decrease of reflectivity of InN nanorods at the wavelength below 1500 nm can be explained by o the collective behavior of electrons and holes above the plasma frequency, which is consistent with the value of ω_p=199 THz obtained by Drude-Smith model.

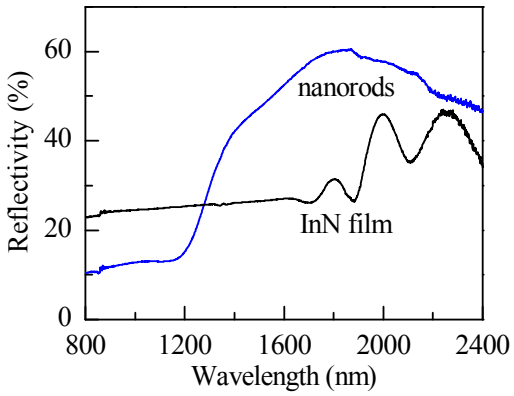

Fig. 5. Near-infrared reflectivity of InN film and nanorods measured at near normal incidence.

A large negative value of backscattering fraction, $c = -0.65$ obtained for InN nanorods means that the localized electrons within the nanorods experience a preferential backward scattering due to electron scatting from defects in InN nanorods caused by the increased structural disorders,[12] or a Coulombic restoring force from charged defects.[22] With the knowledge of the value of c in the Drude-Smith model, it is possible to deduce the electron mobility from the relation,

$$\mu_m = (1+c)(e\tau_0/m^*), \tag{5}$$

which requires the exact value of the effective mass m^* of the InN nanorods. However, up to now no reasonable value of m^* of the pure InN nanorod is available in the literature. Our recent work showed that InN nanorod arrays possess the crystal properties similar to wurtzite InN single crystal[12] and from previously measured near-infrared photoluminescence and room-temperature polarized-Raman scattering data,[23] the carrier density of the InN nanorods is predicted to be ~1.5×10^{19} cm^{-3}. Therefore, we assume that N vs. m^* relation of the InN nanorods is following the same relation of InN single crystal. The effective mass of 0.10 m_0 corresponding to the carrier density 1.5×10^{19} cm^{-3} is then estimated from the N vs. m^* relation calculated by the Kane's two-band $\boldsymbol{k\cdot p}$ model combined with band normalization effect.[24] Using this estimated m^* and the best fit parameters to the Drude-Smith model, an electron mobility of 80±5 cm^2/Vs with an electron density of $4.9\pm0.2\times10^{19}$ cm^{-3} is obtained for the InN nanorod array. The electron mobility of nanostructures could not be obtained by the conventional electron Hall effect measurement method due to the difficulty in making metal contact on the rods. The other traditional mobility measurement techniques include the time-of-flight techniques and various techniques to deduce the mobility from devices. All of these techniques generally have relatively extensive sample preparation procedures, and some of these methods have very limited applicability. It makes THz-TDS a superior method to estimate the carrier mobility of nanostructured materials non-destructively.

The reduced dc conductivity in the Drude-Smith model is given by $\sigma(\omega=0)=(1+c)(eN\mu)$. Since the separation between the InN nanorods is of the order of the nanorod lateral size, inter-rod transport due to the electronic coupling between isolated nanorods may be prohibited. Therefore, the observed reduced mobility of the InN nanorods could be attributed to the intra-rod transport of electrons within the nanorods. A large negative value of $c = -0.65$ obtained for InN nanorods thus indicates that the degree of backscattering of electrons increases due to the confinement of carriers inside a cylindrical nanorod. This value is much larger than that of nanostructures with the lateral sizes of the order of few nm, of which c is very close to –1. Meanwhile, the measured carrier scattering time of 13 fs for the InN nanorods corresponds to the electron mean free path of ~ 2 nm at room temperature, which is much smaller than the average radius of the InN nanorods. Therefore, carriers in the InN nanorods with the average radius of 65 nm can possibly undergo several Drude-

like scattering before preferentially backscattered by the defect centers. And our large value of *c* may correspond to the averaged effect of two scattering mechanisms.

4. ENHANCEMENT OF LIGHT EXTRATION EFFICIENCY

4.1 THz emission mechanism of InN nanorods

InN has the great advantages as THz emitter, such as the low intervalley scattering rate and the narrow bandgap energy (~ 0.7 eV) which can be easily integrated with a compact fiber laser. Despite of its proposed advantages, THz radiation from InN film is typically one order of magnitude weaker than that from InAs, one of the best THz emitting narrow band semiconductors. For the optical light emitting systems, nanostructured nitrides have been heavily studied as a candidate for an efficient light emitter with higher external extraction efficiency. Similarly, due to the increased effective emitting surface area, nanostructured InN is also expected to emit stronger THz signal than the epilayer. The rod size dependence of enhancement has been studied by employing two nanorod samples, LT-NR and HT-NR with different average rod diameters and aerial density.

Figure 6(a) shows the time-domain waveforms of THz emission for LT-NR (black line), HT-NR (red line), and the InN epilayer (blue line), respectively under the photoexcitation of 0.72 mJ/cm^2. As it is expected, LT-NR emits much higher THz wave than InN film and the enhancement is as high as three times in amplitude and ten times in intensity. However, HT-NR with much higher aerial density and aspect ratio emits the similar level of THz waves than that of InN film. The abnormal behavior of HT-NR can be also observed in the pump power dependence of peak amplitude of THz emission. In Fig. 6(b), LT-NR shows the fast increase of THz emission with the photoexcitation energy, while HT-NR shows the similar slow increase of emission to InN film. In any case, all three samples do not show the emission saturation up to the photoexcitation of 1 mJ/cm^2.

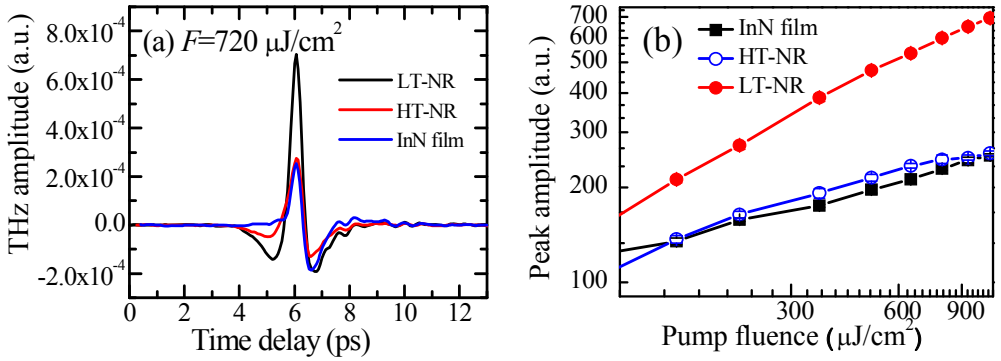

Fig. 6 (a) Emitted THz waveform from LT- and HT-NR and InN film and (b) The peak value of THz waveform vs. the fluence of photoexcitation pulses

THz radiation from the narrow bandgap semiconductors photoexcited by femtosecond laser pulses is known to be due to the ultrafast-laser-driven accelerated carriers formed in a shallow surface area. Therefore, efficient THz emission from these materials is closely related to the near-surface characteristics of the materials, including their morphology, point defects, and the effective surface area. For InN film, since the surface accumulation layer is typically very thin (~ 10 nm) compared to the penetration depth of the laser pulse, its contribution to the total THz radiation is negligibly small compared to the photo-Dember effect. Moreover, for *n*-type InN grown along the *c*-axis, the direction of surface field is perpendicular to the surface and is opposite to the photo-Dember field. And consequently it reduces the total magnitude of THz radiation from *n*-type InN. Room-temperature polarized Raman spectroscopic studies[23] showed that the free carrier concentration in nanorods are one order of magnitude higher than that in the InN film, suggesting that there are a considerable amount of structural defects in the LT-NR. Furthermore, room-temperature photoluminescence (PL) signals of HT-NR and LT-NR are about one to two orders of magnitude lower than that of the InN film.[12] This phenomenon has been attributed to strong surface electron accumulation effect, which screens photocarriers and in turn reduces the radiative recombination in InN nanorods. In the separately measured time-resolved THz spectroscopy measurement, we have observed an extremely slow carrier recombination time (> 5 ns), which is due to the reduced diffusive motion of carriers near the nanorod surfaces.[25]

Nanorods have drastically increased effective surface area compared to the film and due to the obliquely incident photoexcitation laser pulses, the large surface of sidewalls of nanorods may participate in optical absorption as well. The spectral response of reflectance in Fig. 5 shows that at 800 nm, the wavelength of pump laser pulses, absorption in LT-NR is much higher than that in the film. The pump power dependence of optical reflectance also shows that over the whole range of excitation fluence, nanorod arrays show lower reflection (corresponds to higher absorption) of optical waves and it can be understood by the fact that the larger surface area of nanorods participates in more efficient optical absorption.[11] Interestingly, HT-NR has the same level of optical absorption as LT-NR and it is contradict to the observed lower THz emission from HT-NR than that from LT-NR. The penetration depth of the laser pulse in nanostructures depends on the rod distribution so that the surface-to-volume ratio of nanorods becomes the crucial factor for the optical absorption and the corresponding THz emission. The contribution of photoexcited carriers in Si substrate due to the penetrated pump light through the gaps between nanorods is ignored here since HT-NR with much higher rod density show the same level of optical absorption as LT-NR with large void density between nanorods.

The surface field in the thin accumulation layer (~ 10 nm) of unintentionally doped *n*-inN is opposite to the photo-Dember field and thus reduces the THz emission within this layer. For large-size nanorods, reduction of THz emission due to this screening is not significant since the radius of nanorods (65 nm) is much larger than 10 nm. For the ultra-small nanorods in HT-NR, however, the radius of nanorods is comparable to the thickness of the accumulation layer so that the effective surface and volume for THz emission is dramatically reduced. Under the assumption that THz emission from surface accumulation layer is negligible because of screening, we can roughly calculate the effective volume of THz emission by the nanorods solely due to the photo-Dember effect. Comparing with LT-NR, the number of large-size nanorods of HT-NR reduces by ~ 40 %), while there is about three times more number of ultra-small nanorods with small effective volume closely packing the space between large-size nanorods. Therefore, although there are much more nanorods including both large-size and ultra-small rods, the total effective volume of THz emission for HT-NR is about twice smaller than that for LT-NR and it can partially explain the power enhancement of THz emission only from LT-NR.

4.2 THz emission mechanism of *a*-plane InN film

The performance of short-wavelength optoelectronic devices realized by III-nitrides grown along the *c*-axis closely depends on the polarization-induced internal electric fields. These fields are due to piezoelectric and spontaneous polarizations and the strain-dependent piezoelectric polarization along the *c*-axis ([0001]) of the wurtzite crystals increases with the lattice mismatch in the nitride layers.For the layers grown along *a*- (<11-20>) or *m*-axis (<-1100>) direction, polarization-induced electric field perpendicular to the layer interface can be minimized and the efficiency of the devices can be increased. Typically, extraction of THz radiation from the semiconductor surface is limited by the small emission cone. For the InN grown along *c*-axis, THz field due to the photo-Dember effect is perpendicular to the surface so that the light extraction out of surface can be even smaller. Therefore, if the surface electric field can be rotated to be parallel to the surface, one can expect a dramatic increase of light extraction efficiency. In the following, we compare the THz emission from InN films grown along *c*- (polar) and *a*-axis (nonpolar). For nonpolar InN, the absence of electron accumulation layer has been predicted and experimentally confirmed,[26,27] and even if there is, its contribution to the total amount of THz emission can be negligibly small.

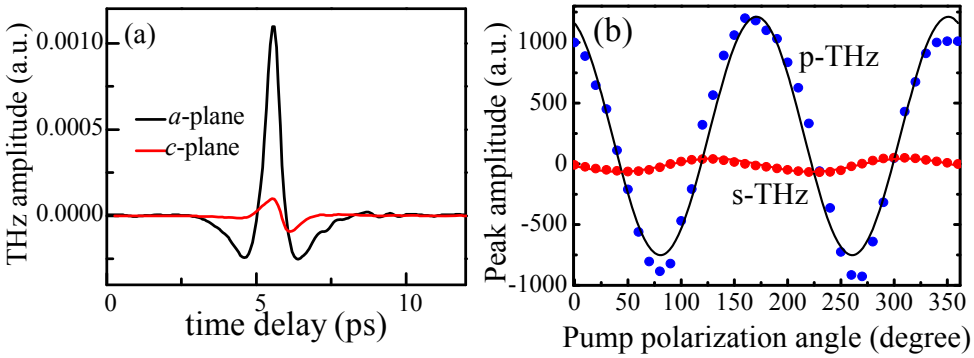

Fig. 7. (a) Comparison of THz waveform emitted from *c*- and *a*-plane InN films. (b) Pump polarization dependence of *p*- and *s*-polarized THz pulses. 90° corresponds to *p*-polarized pumping.

Figure 7(a) shows the maximum amplitude of *p*-polarized THz field from the nonpolar InN film, compared to that from the polar InN film. Under the same *p*-polarized pump fluence at ~0.24 mJ/cm^2, the amplitude of *p*-polarized THz component from nonpolar InN is at least 10 times stronger than that from polar InN. It corresponds to a hundred times of enhancement in intensity and it is one order of magnitude stronger compared to the emission from the nanorods. The pump fluence dependence was measured at the crystal orientation which gives the maximum emission and for both nonpolar and polar InN, the saturation of the emission is not observed for pump fluence up to 1 mJ/cm^2. Figure 7(b) shows the pump polarization dependence of the *p*- and *s*-polarized THz field. As it can be seen clearly in the figure, the emitted THz wave is nearly linearly polarized. The strong *p*-polarized THz beam is generated depending on the polarization state of optical pump, while *s*-polarized component of THz wave is very small for any polarization state of optical pump pulses. The maximum amplitude ratio between *p*- and *s*-polarized components of THz wave is > 10^3 under the *p*-polarized optical pumping.

Another significant difference in THz emission response between polar and nonpolar InN could be observed in its azimuthal angle dependence. The azimuthal angle dependence of *p*- and *s*-polarized THz fields is measured as the InN samples are rotated about the surface normal. Each sample is excited at the pump fluence of ~0.32 mJ/cm^2. The *p*-polarized THz field (blue circles) of nonpolar InN in Fig. 8 shows a large angle-independent field modulated by a weak, but apparent angle-dependent components. For polar InN, no significant angular dependence (<5% of total amplitude) is observed. Usually, azimuthal angle dependent THz emission is attributed to nonlinear optical mechanisms. However, nonlinear optical mechanisms, such as resonance-enhanced optical rectification for the *c*-plane InN[28] under very high excitation fluence (>2 mJ/cm^2), may not have significant contribution for our measurement since the observed pump fluence dependence of terahertz radiation is linear up to 1 mJ/cm^2. It reveals that our pump fluence (0.2-0.35 mJ/cm^2) is well below the regime of photocarrier saturation. A similar fourfold azimuthal angle dependence has been observed for weakly-excited (100) InAs under an external magnetic field, which is proposed to be due to an anisotropic intervalley scattering in four equivalent directions.[29] However, the intervalley scattering for InN is known to be very small so that its contribution can be negligible. In order to clarify the azimuthal angle dependence of emission, azimuthal angle dependent second harmonic generation as well as THz emission from nonpolar InN was simultaneously measured. The solid lines in Fig. 8 are obtained by the best fitting of an analysis based on the bulk and surface second order susceptibility tensor elements of sample and further comprehensive analysis will be published elsewhere.[30] At this point, we will mainly focus on the large constant component of *p*-polarized THz emission from nonpolar InN.

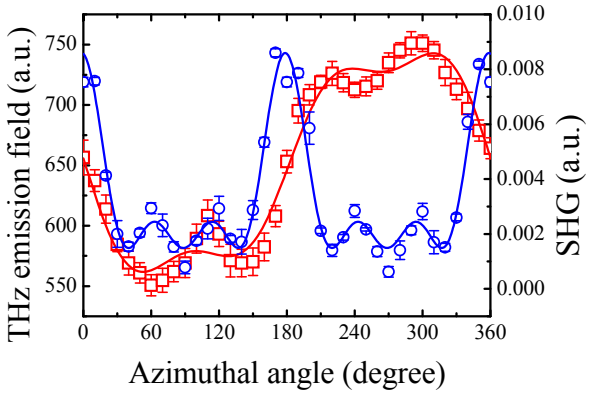

Fig. 8 Azimuthal angle dependence of peak amplitude of THz emission and second harmonic generation signal from nonpolar InN film.

It is known that photoexcited carriers generated close to the surface of semiconductors can be accelerated by an appropriate electric field and the resultant transient electric dipole can lead to generation of THz pulses. The proper electric field can be provided either externally by separate electrodes in photoconductive antennas or internally by the photo-Dember field or the electron accumulation field. The contribution of electron accumulation field to THz emission can be very small for both polar and nonpolar InN due to the narrow thickness of the electron accumulation layer. For the photo-Dember effect, which is proportional to electron mobility and is independent to the crystal growth direction, its contribution to the radiation from nonpolar InN (μ=298 cm^2/V) can be even smaller than that from polar InN (μ=1036 cm^2/V). Therefore, the drastic power enhancement observed for nonpolar InN cannot be explained by either the electron accumulation or the photo-Dember fields. This enhancement, however, is comparable or even larger than that observed by applying a magnetic field parallel to a planar semiconductor surface.[15-17] For a dipole oriented perpendicular to the

surface, only ≤ 1% of the radiated THz power from this dipole can escape the surface because of the small emission cone limited by the total reflection within a material of high refractive index.[31] A magnetic field can rotate the direction of moving charges with respect to semiconductor surface and result as much as two orders of magnitude of power enhancement. Therefore, if the terahertz dipole is formed in the favorable in-plane direction, the same order of power enhancement can be expected.

The stacking sequence of polar InN is *ABABAB*··· along the wurtzite *c*-axis direction so that the surface layers of polar InN have either an In- or a N-terminated polar surfaces. Therefore, the electric field generated by these In-N bilayers directs perpendicular to the surface and the resultant out-of-surface radiation can be significantly limited by the geometrical reason mentioned above. On the other hand, the layers of nonpolar InN have the same number of In and N atoms in a plane and these in-plane In-N dimers form in-plane intrinsic electric field perpendicular to the *a*-axis. The highly photoexcited carriers can then be efficiently coupled to the in-plane electric field such that a more favorable part of emission can escape the emission cone. The power enhancement from nonpolar InN only depends on the growth direction of sample and it can be a universal phenomenon for semiconductors grown in the nonpolar direction.

5. SUMMARY

We have suggested and proved the effective methods of THz power enhancement from InN films and nanorods. THz emission from InN nanorods can be about ten times stronger than that from InN thin film, which depends on the details of nanostructures such as rod diameter. Nonpolar InN film grown along the *a*-axis direction can emit at least a hundred times stronger THz wave than polar InN film. This enhancement rate is comparable to the power enhancement rate from the semiconductors under a strong external magnetic field. Our results suggest that the increase of overlap between the internal radiation pattern and the emission cone is responsible for the enhancement from nonpolar InN film. From the THz-TDS measurement, we could obtain the dielectric response of InN film and nanostructures. It is particularly important to note that the electrical properties (carrier mobility, for example) of nanostructures can be uniquely determined by a spectroscopic measurement in THz range and it can provide the valuable information for further device development.

REFERENCES

[1] Davydov V. Yu., Klochikhin A. A., Seisyan R. P., Emtsev V. V., Ivanov S. V., Bechstedt F., Furthmüller J., Harima H., Mudryi A. V., Aderhold J., Semchinova O., and Graul J., "Absorption and emission of hexagonal InN: Evidence of narrow fundamental band gap", Phys. Status Solidi B **229**, R1–R3 (2002).

[2] Bhuiyan A. G., Hashimoto A., and Yamamoto A., "Indium nitride (InN): A review on growth, characterization, and properties", J. Appl. Phys. **94**, 2779–2808 (2003).

[3] O'Leary S. K., Foutz B. E., Shur M. S., Bhapkar U. V., and Eastman L. F., "Electron transport in wurtzite indium nitride", J. Appl. Phys. **83**, 826–829 (1998).

[4] Foutz B. E., O'Leary S. K., Shur M. S., and Eastman L. F., "Transient electron transport in wurtzite GaN, InN, and AlN", J. Appl. Phys. **85**, 7727–7734 (1999).

[5] Tsen K. T., Poweleit C., Ferry D. K., Lu H., and Schaff W. J., "Observation of large electron drift velocities in InN by ultrafast Raman spectroscopy", Appl. Phys. Lett. **86**, 222103 (2005).

[6] Ahn H., Shen C.-H., Wu C.-L., and Gwo S., "Spectroscopic ellipsometry study of wurtzite InN epitaxial films on Si(111) with varying carrier concentrations", Appl. Phys. Lett. **86**, 201905 (2005).

[7] Honsberg C., Jani O., Doolittle A., Trybus E., Namkoong G., Ferguson I., Nicole D., Payne A., "InGaN–A new solar cell material", Proc. of European Photovoltaic Solar Energy Conference, **15**, 7-11 (2004).

[8] Ascazubi R., Wilke I., Denniston K., Lu H. L., and Schaff W. J., "Terahertz emission by InN," Appl. Phys. Lett. **84**, 4810 (2004).

[9] Pradarutti B., Matthaus G., Bruckner C., Riehemann S., Notni G., Nolti S., Cimalla V., Lebedev V., Ambacher O., and Tunnermann A., "InN as THz emitter excited at 1060 nm and 800 nm, " Proc. of SPIE vol. 6194, 619401 (2006).

[10] Chern G. D., Readinger E. D., Shen H., Wraback M., Gallinat C. S., Koblmuller G., and Speck J. S., "Excitation wavelength dependence of terahertz emission from InN and InAs," Appl. Phys. Lett. **89**, 141115 (2006).

[11] Ahn H., Ku Y.-P., Wang Y.-C., Chuang C.-H., Gwo S., and Pan C.-L., "Terahertz Emission from Vertically Aligned InN Nanorod Array," Appl. Phys. Lett. **91**, 132108 (2007).

[12] Shen C.-H., Chen H.-Y., Lin H.-W., Gwo S., Klochikhin A. A., and Davydov V. Yu., "Near-infrared photoluminescence from vertical InN nanorod array grown on silicon: Effects of surface electron accumulation layer", Appl. Phys. Lett. **88**, 253104 (2006).
[13] Gwo S., Wu C.-L., Shen C.-H., Chang W.-H., Hsu T.-M., Wang J.-S., and Hsu J.-T., "Heteroepitaxial growth of wurtzite InN films on Si(111) exhibiting strong near-infrared photoluminescence at room temperature", Appl. Phys. Lett. **84**, 3765–3767 (2004).
[14] Johnston M. B., Whittaker D. M., Dowd A., Davies A. G., Linfield E. H., Li X., and Ritchie D. A., "Generation of high-power terahertz pulses in a prism", Opt. Lett. **27**, 1935-1937 (2002).
[15] Zhang X. C., Liu Y., Hewitt T. D., Sangsiri T., Kingsley L. E., and Weiner M., "Magnetic switching of terahertz beam", Appl. Phys. Lett. **62**, 2003 (1993).
[16] Gu P., Tani M., Kono S., Sakai K., and Zhang X. C., "Study of terahertz radiation from InAs and InSb", J. Appl. Phys. **91**, 5533 (2002).
[17] Howells S. C., Herrera S. D., and Schlie L. A., "Infrared wavelength and temperature dependence of optically induced terahertz radiation from InSb", Appl. Phys. Lett. 65, 2946 (1994).
[18] Lu H., Schaff W. J., Eastman L. F., Wu J., Walukiewicz W., Cimalla V., and Ambacher O., "Growth of a –plane InN on r-plane sapphire with a GaN buffer by molecular-beam epitaxy", Appl. Phys. Lett. **83**, 1136 (2003).
[19] Kasic K., Schubert M., Satio Y, Nanishi Y., and Wagner G, "Effective electron mass and phonon modes in *n*-type hexagonal InN", Phys. Rev. B **65**, 115206 (2002).
[20] Garcia-Vidal F.J., Pitarke J. M., and Pendry J. B., "Effective medium theory of the optical properties of aligned carbon nanotubes", Phys. Rev. Lett. **78**, 4289 (1997).
[21] Smith N. V., "Classical generalization of the Drude formula for the optical conductivity", Phys. Rev. B **64**, 155106 (2001)
[22] Baxter J. B. and Schmuttenmaer C. A., "Conductivity of ZnO nanowires, nanoparticles, and thin films using time-resolved terahertz spectroscopy", J. Phys. Chem. B **110**, 25229 (2006).
[23] Chen H.-Y., Shen C.-H., Lin H.-W., Chen C.-H., Wu C.-Y., Gwo S., Davydov V. Yu., and Klochikhin A. A., "Near-infrared photoluminescence of vertically aligned InN nanorods grown on Si(111) by plasma-assisted molecular-beam epitaxy", Thin Solid Films, **515**, 961 (2006).
[24] Fu S. P. and Chen Y. F., "Effective mass of InN epilayers", Appl. Phys. Lett. **85**, 1523 (2004).
[25] Ahn H., Chuang C.-H., Ku Y.-P., and Pan C.-L., "Free carrier dynamics of InN nanorods investigated by time-resolved terahertz spectroscopy," accepted for publication in J. Appl. Phys. (2009).
[26] van de Walle C. G. and Segev D., "Microscopic origins of surface states on nitride surfaces", J. of Appl. Phys. **101**, 081704 (2007).
[27] Wu C.-L., Lee H.-M., Kuo C.-T., Chen C.-H., and Gwo S., "Absence of Fermi-level pinning at cleaved nonpolar InN surfaces", Phys. Rev. Lett. **101**, 106803 (2008).
[28] Reid M. and Fedosejevs R., "Terahertz emission from (100) InAs surfaces at high excitation fluences", Appl. Phys. Lett. **86**, 011906 (2005).
[29] Estacio E., Sumikura H., Murakami H., Tani M., Ponceca C., Pobre Jr. R., Quiroga R., and Ono S., "Magnetic-field-induced fourfold azimuthal angle dependence in the terahertz radiation power of (100) InAs", Appl. Phys. Lett. **90**, 151915 (2007).
[30] Ahn H., Yu K.-J., and Gwo S., in preparation.
[31] Johnston M. B., Whittaker D. M., Corchia A., Davies A. G., and Linfield E. H., "Simulation of terahertz generation at semiconductor surfaces", Phys. Rev. B **65**, 165301 (2002).